Pràctica 2: Reacció - Difusió (Meinhardt)

Introducció.

El "matoll tigre" (*tiger bush*) és un tipus de planta que es troba en climatologia semi-àrida i que s'organitza en bandes alternades de matoll i terra sense (o molt poca) vegetació, situats en terrenys amb un cert grau d'inclinació. Aquests patrons es formen com a conseqüència de l'interacció de diferents mecanismes. La manca d'aigua no permet que el matoll s'estengui per tota la superfície del terreny uniformement. L'aigua llisca per la pendent i es recol·lectada per les plantes que han aconseguit prosperar. Aquests patrons depenen de les condicions climàtiques (p.ex: precipitacions) i de la capacitat de colonització del matoll (difusió).

Objectius

En aquesta pràctica simularem la formació de *tiger bush* amb un model molt senzill de reacció-diffusió (veure C. A. Klausmeier, *"Regular and Irregular Patterns in Semiarid Vegetation"* **Science** 284 (5412), 1826 (1999)). A cada patch simulem la dinàmica de les *concentracions* d'aigua (variable 'w') i matoll (variable 'p') descrites per les següents equacions diferencials:

$$\frac{\partial w}{\partial t} = a - wp^2 + v\frac{\partial w}{\partial y}$$

$$\frac{\partial p}{\partial t} = wp^2 - mp - D\left(\frac{\partial p}{\partial x} + \frac{\partial p}{\partial y}\right)$$

on el paràmetre D=0.1 indica la velocitat de propagació del matoll als 4 *patches* veïns, a=2 és la taxa de precipitacions, m =0.45 és la mortalitat espontània de la planta. La interfície del programa en Netlogo es com la següent pantalla:
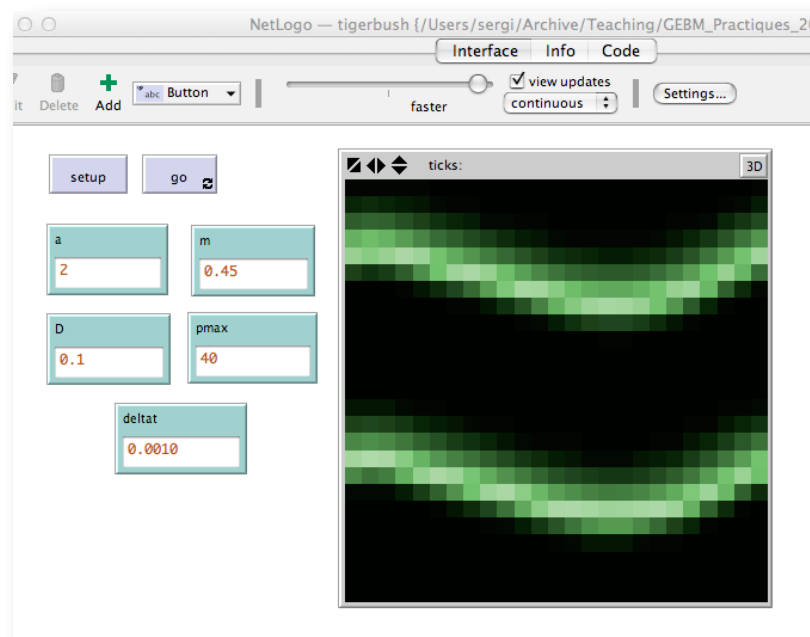
Apartat 1: Escriure el programa que simula el model de formació de Tiger bush amb les paràmetres indicats anteriorment. El pas d'integració és deltat = 0.001.

Apartat 2: Descriure quin és el comportament d'aquest sistema al variar el coeficient de diffusió D = {0, 0.1, 0.5, 0.8}. Després, fixar el coeficient de difusió de la planta D = 0.1 i explorar l'espai de paràmetres a = {1.1, 1.2, 1.3, 1.4, 1.5, 1.5, 1.6, 1.7, 1.8, 1.9, 2} i m = {0.1, 0.2, 0.3, 0.4, 0.5, 0.6}. Crear una taula on es pugui veure el resultat dels paràmetres, com la següent:
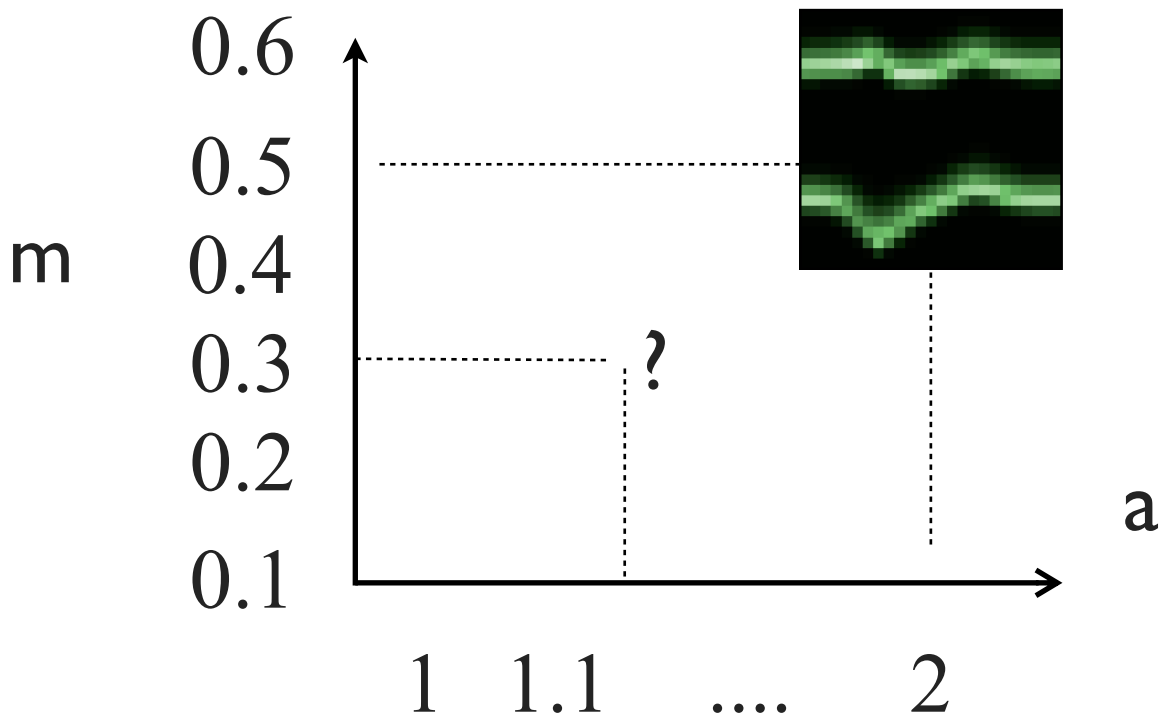
site (*24*)]. Thus, $\delta^{11}B_{sw}$ is estimated at 40.6 per mil, and disregarding the $\delta^{11}B$ value for *M. crassata*, $pH_{best} = 8.05$.

Two of four key chemical variables [pCO_2, pH, the total alkalinity ($\Sigma_{alkalinity}$), and the total dissolved inorganic carbon (ΣCO_2)] are required to define the thermodynamics of the CO_2 system in the ocean (*31*). As we only have an estimate of paleo-pH from our Eocene sample, pCO_2 can only be calculated as a function of one of the other two key variables (*32*) (Fig. 3). Assuming that ΣCO_2 values were the same as the modern ocean, for pH_{min} of 7.91 we calculate pCO_2 as 530 to 570 ppm. To achieve a value of five times modern pCO_2 we would have to invoke ΣCO_2 concentrations of more than twice the modern value, which is unreasonable because it would imply a larger variation in calcium carbonate saturation in the oceans than is compatible with the geologic record (*33*). Assuming pH_{max} for our sample of 8.33 and modern ΣCO_2 concentrations, we obtain a minimum estimate of pCO_2 of 170 to 190 ppm. Our pH_{best} estimate of 8.05 with modern ΣCO_2 gives a pCO_2 of 370 to 400 ppm, only slightly higher than modern concentrations.

Seasonal temperature cycles and biological processes mean that the pCO_2 of seawater in the surface mixed layer is not in perfect equilibrium with the atmosphere, but this deviation is generally <10% in the absence of upwelling of CO_2-rich deep waters (*31*). As our sample splits were not taken from an upwelling area and represent the average pH recorded by many individuals that lived at different times, the calculated pCO_2 values give reasonable estimates of the mid-Eocene atmosphere, provided ΣCO_2 was not greatly different from the modern value. If our estimate of middle Eocene pCO_2 is correct, then it implies either that Earth's climate is very sensitive to small changes in pCO_2, or that the global cooling since the Eocene was not driven primarily by changes in pCO_2, but rather reflects reorganization of ocean circulation resulting from tectonic opening and closing of oceanic gateways (*2*).

References and Notes

1. K. G. Miller, R. G. Fairbanks, G. S. Mountain, *Paleoceanography* **2**, 1 (1987).
2. J. P. Kennett, *Marine Geology* (Prentice-Hall, Englewood, NJ, 1982), p. 695.
3. R. A. Berner, A. C. Lasaga, R. M. Garrels, *Am. J. Sci.* **283**, 641 (1983).
4. E. J. Barron, *Palaeogeogr. Palaeoclimatol. Palaeoecol.* **50**, 45 (1985).
5. M. E. Raymo and W. F. Ruddiman, *Nature* **359**, 117 (1992).
6. W. A. Berggren and D. R. Prothero, in *Eocene-Oligocene Climatic and Biotic Evolution*, D. R. Prothero and W. A. Berggren, Eds. (Princeton Univ. Press, Princeton, NJ, 1992), p. 1.
7. R. M. Owen and D. H. Rea, *Science* **227**, 166 (1985).
8. D. K. Rea *et al.*, *Palaeogeogr. Palaeoclimatol. Palaeoecol.* **79**, 117 (1990).
9. O. Eldholm and E. Thomas, *Earth Planet. Sci. Lett.* **117**, 319 (1993).
10. D. M. Kerrick and K. Caldeira, *Chem. Geol.* **145**, 213 (1998).
11. J. C. Zachos *et al.*, *J. Geol.* **101**, 191 (1993).
12. M. A. Arthur *et al.*, *Eos* **72**, 166 (1991).
13. P. V. Brady, *J. Geophys. Res.* **96**, 18101 (1991).
14. K. H. Freeman and J. M. Hayes, *Global Biogeochem. Cycles* **6**, 185 (1992).
15. T. R. Worsley *et al.*, *Geol. Soc. Am. Spec. Pap.* **288**, 57 (1994).
16. J. C. McElwain, *Philos. Trans. R. Soc. London Ser. B* **353**, 83 (1998).
17. R. A. Berner, *Am. J. Sci.* **291**, 339 (1991).
18. T. E. Cerling, *ibid.* **293**, 377 (1993).
19. R. A. Berner, *ibid.* **294**, 56 (1994).
20. Boron exists as two main species in seawater, $B(OH)_3$ and $B(OH)_4^-$, the relative abundance of which is controlled primarily by pH [J. F. Hershey, M. Fernandez, P. J. Milne, F. J. Millero, *Geochim. Cosmochim. Acta* **50**, 143 (1986)]. There is a strong isotopic fractionation between the two species, in which ^{10}B prefers tetrahedral coordination by about -19.8 per mil relative to ^{11}B (*29*). On the basis of analysis of a variety of modern marine carbonates, N. G. Hemming and G. N. Hansen [*ibid.* **56**, 537 (1992)] suggested that boron incorporation into carbonate is from $B(OH)_4^-$ and consequently that the $\delta^{11}B$ of calcite is a pH indicator. A. J. Spivack, C. F. You, and H. J. Smith [*Nature* **363**, 149 (1993)] suggested that boron isotope measurements of seawater pH could be used to infer past pCO_2. The pH relation was tested by A. Sanyal *et al.* [*Paleoceanography* **11**, 513 (1996)] using the living planktonic foraminifer *Orbulina universa*, batches of which were cultured from the juvenile stage to maturity over a controlled range of pH conditions. This experiment confirmed the predicted relation between the $\delta^{11}B$ of shell calcite and pH, except that a consistent offset from the expected $\delta^{11}B$ value of -4 per mil was observed. Sanyal and others interpreted this offset as a probable vital effect. It may have been caused by dissolution of previously formed calcite in *O. universa* as it constructs its final chamber. Further work by A. Sanyal, N. G. Hemming, W. S. Broecker, and G. N. Hanson [*Global Biogeochem. Cycles* **11**, 125 (1997)] suggests that the offset is peculiar to *O. universa* and that other species construct their shells at or close to equilibrium $\delta^{11}B$ of $B(OH)_4^-$. The value of $\delta^{11}B$ is calculated as follows:

$$\delta^{11}B = \left[\frac{(^{11}B/^{10}B)_{sample}}{(^{11}B/^{10}B)_{standard}} - 1 \right] \times 1000$$

where $(^{11}B/^{10}B)_{standard} = 3.9873$ for the standard NBS SRM 951.
21. M. R. Palmer, P. N. Pearson, S. J. Cobb, *Science* **282**, 1468 (1998).
22. T. J. Bralower *et al.*, *Paleoceanography* **10**, 841 (1995).
23. A. Boersma, I. Premoli Silva, N. J. Shackleton, *ibid.* **2**, 287 (1987).
24. P. N. Pearson, N. J. Shackleton, M. A. Hall, *J. Foraminifer. Res* **23**, 123 (1993).
25. A. J. M. van Eijden, *Palaeogeogr. Palaeoclimatol. Palaeoecol.* **113**, 267 (1995).
26. G. Lu and G. Keller, *J. Foraminiferal. Res.* **26**, 103 (1996).
27. P. N. Pearson, *Paleontol. Soc. Pap.* **4**, 138 (1998).
28. F. J. Millero, *Geochim. Cosmochim. Acta* **59**, 661 (1995).
29. H. Kakihana *et al.*, *Bull. Chem. Soc. Jpn.* **50**, 158 (1977).
30. P. M. Kroopnick, *Deep Sea Re.* **32**, 57 (1985).
31. W. S. Broecker and T. H. Peng, *Tracers in the Sea* (Columbia Univ. Press, New York, 1982).
32. The partial pressure of carbon dioxide and the concentration of total dissolved inorganic carbon are related by the equation

$$pCO_2 = K_H \left(1 + \frac{K_1}{[H^+]} + \frac{K_1 K_2}{[H^+]^2} \right)^{-1} \Sigma CO_2$$

where K_H is the Henry's law constant for CO_2, and K_1 and K_2 are the first and second dissociation constants for carbonic acid.
33. T. J. van Andel, *Earth Planet. Sci. Lett.* **26**, 187 (1975).
34. Supported by a grant from the Natural Environment Research Council. The sample used in this research was supplied by the Ocean Drilling Program. We are grateful to S. Cobb for help in sample preparation and to two anonymous reviewers.

27 January 1999; accepted 22 April 1999

Regular and Irregular Patterns in Semiarid Vegetation

Christopher A. Klausmeier

Vegetation in many semiarid regions is strikingly patterned, forming regular stripes on hillsides and irregular mosaics on flat ground. A simple model of plant and water dynamics based on ecologically realistic assumptions and with reasonable parameter values captures both of these types of patterns. The regular patterns result from a Turing-like instability; the irregular patterns arise when the ecological dynamics amplify slight small-scale topographic variability. Because of the close agreement between observations and these theoretical results, this system provides a clear example of how nonlinear mechanisms can be important in determining the spatial structure of plant communities.

Pattern formation has long interested both theoretical biologists (*1*, *2*) and plant ecologists (*3*, *4*). Theoretical studies have shown that local interactions coupled by dispersal can cause nonuniform distributions of organisms to develop in the absence of underlying heterogeneity. Recently it has been shown that such an interaction between a herbivorous insect and its parasitoid localizes outbreaks of the herbivore, in accordance with mathematical models (*5*). However, in general, close agreement between the mathematical theory and observation or experiment has been rare (*6*). Furthermore, most of these studies have focused on interactions between animal populations, not on the interaction of plants and their abiotic resources.

Vegetation patterns are found in many semiarid regions including parts of Africa (*7*–

Department of Ecology, Evolution and Behavior, University of Minnesota, St. Paul, MN 55108, USA. E-mail: klaus@biosci.umn.edu

11), Australia (*12, 13*), and Mexico (*14*). On hillsides, stripes of vegetation alternate with patches of bare ground parallel to the hills' contours (*7–14*) (Fig. 1); on flat ground, stationary irregular mosaics consisting of the same species have been reported (*8, 10*). Because of their distinct appearance, the regular stripes have been more extensively studied than the irregular patterns. Vegetation stripes form under conditions of low rainfall, gentle slope, and on soil on which plants increase water infiltration (*4, 9*). The slight differences between soil within and between stripes are attributable to the vegetation itself (*4, 9*). The plant community composition varies, consisting of grasses in some locations (*7, 10*) and shrubs and trees in others (*11, 15*).

The verbal explanation given for the maintenance of striped vegetation is as follows (*4, 9*): Water does not infiltrate in the bare areas between vegetation stripes, but flows downhill to the next stripe where it can soak in and support plant growth. This water is exhausted by the downhill side of the stripe, which causes the next bare area. The stripes slowly move uphill because colonization of bare areas can occur only at the moister uphill side of the stripe (*14*) and because plants on the downhill side of the stripe die as a result of inadequate water.

The model is a pair of partial differential equations for water (W) and plant biomass (N), defined on an infinite two-dimensional domain indexed by X and Y. Water is supplied uniformly at rate A and is lost due to evaporation at rate LW. Plants take up water at rate $RG(W)F(N)N$, where $G(W)$ is the functional response of plants to water and $F(N)$ is an increasing function that describes how plants increase water infiltration. For simplicity I use the linear functions $G(W) = W$ and $F(N) = N$, but the results are not sensitive to the exact form of these functions. J is the yield of plant biomass per unit water consumed. Plant biomass is lost only through density-independent mortality and maintenance at rate MN. Water flows downhill (in the negative X direction) at speed V. Plant dispersal is modeled by a diffusion term with diffusion coefficient D;

more realistic dispersal kernels can be approximated by a such a term (*2*). Taken together, these assumptions result in

$$\frac{\partial W}{\partial T} = A - LW - RWN^2 + V\frac{\partial W}{\partial X}$$

$$\frac{\partial N}{\partial T} = RJWN^2 - MN + D\left(\frac{\partial^2}{\partial X^2} + \frac{\partial^2}{\partial Y^2}\right)N$$

(1)

Unlike previous phenomenological models of semiarid vegetation (*16*), this model incorporates the water dynamics thought to be responsible for pattern formation. Thus, all results can be interpreted in terms of parameters that have clear biological meanings, and the validity of the proposed water-based mechanism can be assessed. Equations 1 can be nondimensionalized (*17*) to

$$\frac{\partial w}{\partial t} = a - w - wn^2 + v\frac{\partial w}{\partial x}$$

$$\frac{\partial n}{\partial t} = wn^2 - mn + \left(\frac{\partial^2}{\partial x^2} + \frac{\partial^2}{\partial y^2}\right)n$$

(2)

The nondimensionalized model (Eq. 2) has only three parameters: a, which controls water input; m, which measures plant losses; and v, which controls the rate at which water flows downhill.

The first step in analyzing the model is to determine the behavior of the nonspatial model obtained by setting space derivatives equal to zero. The nonspatial model has either one or three equilibria, which correspond to spatially homogeneous equilibria of the full model (Eq. 2). The equilibrium consisting of no plants, $\hat{w} = a$ and $\hat{n} = 0$, always exists and is linearly stable. When $a > 2m$, two nontrivial equilibria exist. One of these is never stable and can be ignored; the other is linearly stable for ecologically relevant parameters (*18*). Thus, the model exhibits multiple stable states, one vegetated and the other bare (*19*).

Returning to the full model (Eq. 2), I examine two cases: hillsides and flat ground. On hillsides, $v \gg 0$. Linear stability analysis can

be used to determine whether regular patterns can form (*2*). This analysis shows that for given mortality rate m and water flow speed v, there is a critical value of water input a below which regular stripes form (Figs. 2 and 3, A and B). This instability is similar to a Turing instability (*1, 2*), but differs in that it results from the interplay between reaction, diffusion, and advection (*20*). One consequence of this difference is that the eigenvalue that determines the instability of the homogeneous equilibrium is complex with a negative imaginary term. This causes the pattern to oscillate in time and the stripes to move uphill. Although the asymptotic state is parallel, evenly spaced vegetation stripes (Fig. 3B), defects in the pattern are present during the transient dynamics. These defects appear as forks between stripes (Fig. 3A) that can be seen in aerial photographs of natural striped vegetation patterns (Fig. 1). These patterns are robust against environmental stochasticity in the form of year-to-year variation in rainfall.

The model is in order-of-magnitude agreement with field observations. Plausible values of the parameters for trees and grass are as follows: $a_{\text{tree}} = 0.077$ to 0.23, $m_{\text{tree}} = 0.045$, $a_{\text{grass}} = 0.94$ to 2.81, $m_{\text{grass}} = 0.45$, and $v = 182.5$ (*21*). Given these parameters, the model predicts tree stripes to have wavelengths from 23 to 67 m and move from 0.4 to 0.6 m year^{-1} and grass stripes to have wavelengths from 8.1 to 28 m and move from 1.4 to 1.9 m year^{-1}. Field observations show that tree stripes vary in wavelength from 70 to 190 m (*8*) and may move from 0.15 to 0.3 m year^{-1} (*11*); grass stripes range in wavelength from 1 to 40 m (*7, 10*) and move from 0.3 to 1.5 m year^{-1} (*7*). Because some parameters were not available in
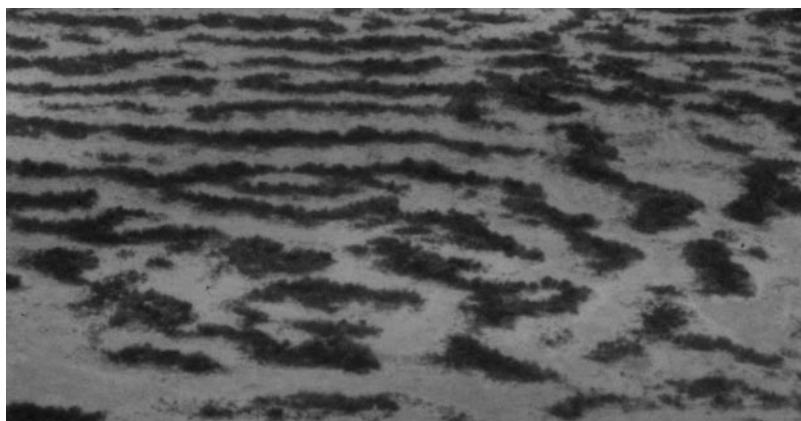

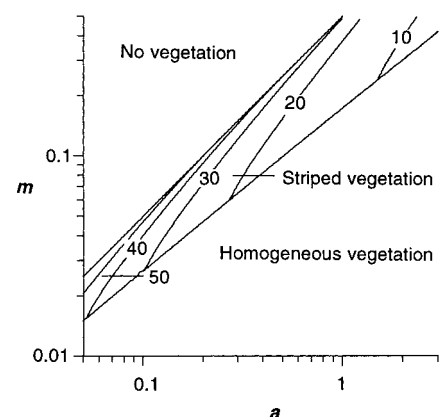**Fig. 1.** Regular vegetation stripes near Niamey, Niger.

Fig. 2. Behavior of the model (Eq. 2) as determined by the water input rate a and plant loss rate m when water velocity $v = 182.5$. The contours give the dimensional stripe wavelength in meters as determined by the most unstable mode found with linear stability analysis. As water input is decreased or plant loss is increased, the model predicts a transition from homogeneous vegetation, to stripes of increasing wavelength, to no vegetation.

Fig. 3. (**A** to **C**) Snapshots of plant densities obtained by numerical solution of the model on a 100 by 100 domain (in dimensional terms, 2500 m²) with periodic boundary conditions. Darker colors indicate higher plant densities. Water flows from positive *x* to negative *x*. $a = 2$, $m = 0.45$. (A and B) On a hillside, $v = 182.5$. An animation of this output is available on *Science* online at www.sciencemag.org/feature/data/990551.shlstripes.qt. (A) During the transient dynamics, defects in the form of forks and dead-ends occur ($t = 100$). (B) Regular stripes on hillsides, after transient dynamics ($t = 1000$).
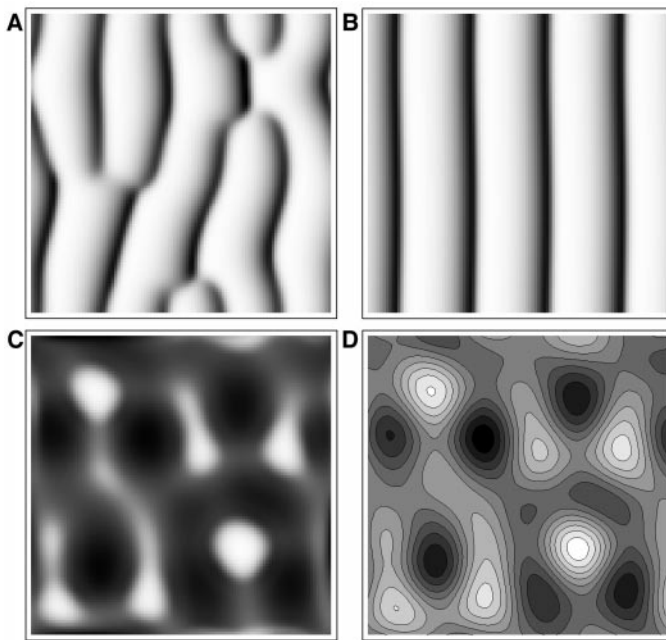
These stripes move uphill at a constant speed. (C) On flat ground with slight topographic variation. Plant density varies 90-fold, from 0.08 to 7.2. (**D**) Elevation in the irregular landscape used in part (C), where darker colors represent lower elevations. The topographic variation is 0.02 times the variation in the evenly sloping landscapes used for (A) and (B). If the slopes used in (A) and (B) are 1:100, then the variation in height in (C) is 1 cm.

the literature, these were set to plausible values. Direct estimation of all the parameters from one field site would allow a more rigorous test of this model. The quantitative fit of the model to data would also be improved by considering a nonlinear facilitation function and functional response, and by separating water into surface and subsurface compartments.

On flat ground, linear stability analysis shows that regular pattern formation is impossible when the spatially homogeneous equilibrium is stable in the nonspatial model. Numerical solution of the model (Eq. 2) shows that irregular patterns due to spatial chaos and spiral waves can arise for parameter values for which the nonspatial model has a stable limit cycle or is excitable (*22*), but these parameters are ecologically unrealistic (*18*). Although this system exhibits multiple stable states, this cannot account for the irregular patterns because a patch of vegetation expands as a traveling wave (*2*). A potential explanation for the irregular mosaics is that slight topographic variation can lead to large variation in plant density (Fig. 3, C and D). Higher ground is left bare whereas lower points support dense vegetation. The ecological dynamics amplify the underlying heterogeneity into a sharply differentiated mosaic. This hypothesis is supported by Belsky's observation that water flows from sparsely to densely vegetated patches in a grassland mosaic (*10*). A simple experimental test of this mechanism would be to level the bare phase of an irregular mosaic and see whether the vegetated phase expands.

This model can be used to help understand the influence of rainfall and grazing on semiarid vegetation. Linear stability analysis shows that the wavelength of the regular patterns increases with decreasing water input, *a* (Fig. 2), as has been reported along geographic gradients in rainfall in natural striped vegetation (*9*) and suggested as an indicator of ecosystem degradation (*13*). Increased grazing can be considered an additional source of mortality, increasing the nondimensional parameter *m* through the dimensional parameter *M*. As with decreasing *a*, increasing *m* causes a transition from homogeneous vegetation to striped vegetation of increasing wavelength, to no vegetation (Fig. 2). This explains the observations that intense grazing can cause striped vegetation to be replaced by bare ground (*12, 15*) and that herbivore exclosures can cause mosaics to be replaced by homogeneous vegetation (*10*).

Although it greatly simplifies the physics and biology of these systems, this model is in reasonable agreement with field observations of regular and irregular patterns in semiarid ecosystems. It supports the verbal argument that water-plant dynamics can explain the formation and maintenance of striped vegetation patterns and suggests that irregular mosaics are most likely due to slight topographic variation. These results show that spatial pattern in ecological systems can result from both self-organization and amplification of underlying heterogeneity.

References and Notes

1. A. Turing, *Philos. Trans. R. Soc. London Ser. B* **237**, 37 (1952); L. A. Segel and J. L. Jackson, *J. Theor. Biol.* **37**, 545 (1972).
2. A. Okubo, *Diffusion and Ecological Problems: Mathematical Models* (Springer-Verlag, New York, 1980); J. D. Murray, *Mathematical Biology* (Springer-Verlag, New York, 1989).
3. A. Watt, *J. Ecol.* **35**, 1 (1947).
4. P. Greig-Smith, *ibid.* **67**, 755 (1979).
5. J. L. Maron and S. Harrison, *Science* **278**, 1619 (1997).
6. E. K. Steinberg and P. M. Kareiva, in *Spatial Ecology: The Role of Space in Population Dynamics and Interspecific Interactions*, D. Tilman and P. Kareiva, Eds. (Princeton Univ. Press, Princeton, NJ, 1997), pp. 318–332; P. Turchin, J. D. Reeve, J. T. Cronin, R. T. Wilkens, in *Modeling Spatiotemporal Dynamics in Ecology*, J. Bascompte and R. V. Solé, Eds. (Springer-Verlag, New York, 1998), pp. 199–213.
7. G. A. Worrall, *J. Soil Sci.* **10**, 34 (1959).
8. L. P. White, *J. Ecol.* **58**, 549 (1970).
9. ——, *ibid.* **59**, 615 (1971).
10. A. J. Belsky, *ibid..* **74**, 841 (1986).
11. C. F. Hemming, *ibid.* **53**, 57 (1965).
12. J. A. Mabbutt and F. C. Fanning, *J. Arid Environ.* **12**, 41 (1987).
13. D. J. Tongway and J. A. Ludwig, in *Landscape Ecology, Function and Management: Principles from Australia's Rangelands*, J. Ludwig, D. Tongway, D. Freudenberger, J. Noble, K. Hodgkinson, Eds. (CSIRO, Collingwood, Australia, 1997), pp. 49–61.
14. C. Montaña, J. Lopez-Portillo, A. Mauchamp, *J. Ecol.* **78**, 789 (1990); C. Montaña, *ibid.* **80**, 315 (1992).
15. G. E. Wickens and F. W. Collier, *Geoderma* **6**, 43 (1971).
16. J. M. Thiéry, J.-M. D'Herbès, C. Valentin, *J. Ecol.* **83**, 497 (1995); R. Lefever and O. Lejeune, *Bull. Math. Biol.* **59**, 263 (1997).
17. Let $w = R^{1/2}L^{-1/2}JW$, $n = R^{1/2}L^{-1/2}N$, $x = L^{1/2}D^{-1/2}X$, $y = L^{1/2}D^{-1/2}Y$, $t = LT$, $a = AR^{1/2}L^{-3/2}J$, $m = ML^{-1}$, and $v = VL^{-1/2}D^{-1/2}$.
18. For some parameter values there exist limit cycles in which plants and water oscillate; for others, the trivial equilibrium is excitable. The parameters I estimated (*21*) are far from those that lead to limit cycles and excitability. Both of these behaviors require plants and water to be on similar time scales. Because water changes on a much faster time scale than plant biomass, such parameters are ecologically unrealistic and will not be considered here.
19. M. Rietkerk and J. Van de Koppel, *Oikos* **79**, 69 (1997).
20. J. Jorné, *J. Theor. Biol.* **43**, 375 (1974); A. B. Rovinsky and M. Menzinger, *Phys. Rev. Lett.* **69**, 1193 (1992).
21. Rainfall in semiarid regions $A = 250$ to 750 kg H_2O m^{-2} year^{-1}. I assume that $\hat{W}_{noveg} = 75$ kg H_2O m^{-2} when $A = 300$ kg H_2O m^{-2} year^{-1}. Because $\hat{W}_{noveg} = A/L$, this implies that the evaporation rate $L = 4$ year^{-1}. From A. Mauchamp, S. Rambal, and J. Lepart [*Ecol. Model.* **71**, 107 (1994)], I obtained the following four parameters: $J_{tree} = 0.002$ kg dry mass (kg H_2O)$^{-1}$, $J_{grass} = 0.003$ kg dry mass (kg H_2O)$^{-1}$, $M_{tree} = 0.18$ year^{-1}, and $M_{grass} = 1.8$ year^{-1}. I set $D = 1$ m^2 year^{-1} and V increases from 0 m year^{-1}; in examples I let $V = 365$ m year^{-1}. I obtained values for R from the expression for the equilibrium plant biomass,

$$\hat{N} = \frac{AJ}{2M} + \sqrt{\left(\frac{AJ}{2M}\right)^2 - \frac{L}{R}}$$

assuming $\hat{N}_{tree} = 2.0$ kg m^{-2} and $\hat{N}_{grass} = 0.4$ kg m^{-2} when $A = 300$ kg H_2O m^{-2} year^{-1}. This gives $R_{tree} = 1.5$ kg H_2O m^{-2} year^{-1} (kg dry mass)$^{-2}$ and $R_{grass} = 100$ kg H_2O m^{-2} year^{-1} (kg dry mass)$^{-2}$.
22. M. C. Cross and P. C. Hohenberg, *Rev. Mod. Phys.* **65**, 850 (1993); R. M. May, in *Frontiers in Mathematical Biology*, S. A. Levin, Ed. (Springer-Verlag, New York, 1994), pp. 326-344.
23. I thank P. Abrams, D. Aronson, B. Foster, S. Geritz, C. Lehman, E. Litchman, S. Naeem, C. Neuhauser, M. Pascual, M. Rietkerk, E. Siemann, and D. Tilman for helpful discussion and comments. Photographs supplied by S. Prince (Geography Department, University of Maryland), whose work with HAPEX-Sahel was partly supported by NASA grant NAGW1967. This work was supported by the various fellowships from the University of Minnesota.